Weak-interaction mediated rates on iron isotopes for presupernova evolution of massive stars

Jameel-Un Nabi^{1,2}

PACS 23.40.Bw - Weak interaction and lepton (including neutrino) aspects

PACS 26.50.+x - Nuclear physics aspects of supernovae

PACS 21.60. Jz - Nuclear Density Functional Theory and extensions

Abstract. - During the presupernova evolution of massive stars, the isotopes of iron, ^{54,55,56}Fe, are advocated to play a key role inside the cores primarily decreasing the electron-to-baryon ratio (Y_e) mainly via electron capture processes thereby reducing the pressure support. Electron decay and positron capture on ⁵⁵Fe, on the other hand, also has a consequential role in increasing the lepton ratio during the silicon burning phases of massive stars. The neutrinos and antineutrinos produced, as a result of these weak-interaction reactions, are transparent to the stellar matter and assist in cooling the core thereby reducing the entropy. The structure of the presupernova star is altered both by the changes in Y_e and the entropy of the core material. The aim of this paper is to report the improved microscopic calculation of Gamow-Teller (GT_{\pm}) strength distributions of these key isotopes of iron using the pn-QRPA theory. The main improvement comes from the incorporation of experimental deformation values for these nuclei. Additionally six different weak-interaction rates, namely electron & positron capture, electron & positron decay, and, neutrino & antineutrino cooling rates, were also calculated in presupernova matter. The calculated electron capture and neutrino cooling rates due to isotopes of iron are in good agreement with the large-scale shell model (LSSM) results. The calculated beta decay rates, however, are suppressed by three to five orders of magnitude.

All elements heavier than boron are formed by nuclear reactions inside stars. Core-collapse supernovae are considered to be one of the major contributors to the production of elements in the universe. However, core-collapse simulators, to date, find it challenging to successfully transform the collapse into an explosion. The details of the micro-physics in the prevailing extreme environment is poorly understood. This include but are not limited to the explosion mechanism, role of neutrino interactions, equation of state and the treatment of hydrodynamic instabilities in three dimensional simulations. A mechanism involving transfer of energy from neutrinos has long been favored but other vistas involving rapid rotation and magnetic fields are also being explored. Whereas in the prevailing environment reactions mediated by strong and electromagnetic force are in chemical equilibrium those mediated by the weak interactions are not (the non-thermal neutrinos produced are transparent to the stellar matter for densities up to around $10^{11}gcm^{-3}$) and have a decisive role to play in the intricate dynamics of core-collapse. The weak interaction have several crucial effects in the course of development of a star. These include initiation of the gravitational collapse of the core of massive stars, neutronisation of the core material and formation of heavy elements

¹ Faculty of Engineering Sciences, GIK Institute of Engineering Sciences and Technology, Topi 23640, Swabi, NWFP, Pakistan

² The Abdus Salam ICTP, Strada Costiera 11, 34014, Trieste, Italy

above iron via the r-process.

In order to understand the supernova explosion mechanism and other related astrophysical events of significance international collaborations of astronomers and physicists are being sought. A large amount of useful observational data is now accessible due to space-and ground-based telescopes. Considerable efforts are also being done to determine the equation of state of ultradense matter. State-of-the-art supernova models employ multidimensional modelling making use of sophisticated numerical treatments. This in turn is also made possible by faster computing machines. Reliable determinations of nuclear properties of many nuclei (including neutron-rich unstable nuclide) are becoming available thanks to improved nuclear-mass models coupled with new experimental measurements.

It is highly desirable to calculate the presupernova stellar structure with the most reliable physical data and inputs. The structure of the presupernova star is altered both by the change in Y_e and entropy in its interior. A smaller precollapse iron core mass and a lower entropy should favor an explosion. A smaller iron core size implies less energy loss by the shock in photodisintegrating the iron nuclei in the overlying onion-like structure whereas a lower entropy environment can assist to achieve higher densities for the ensuing collapse generating a stronger bounce and in turn forming a more energetic shock wave [1]. A smaller entropy can also assist in achieving a higher final value of Y_e by reducing the abundance of free protons (which act as a major source of electron sink through electron capture reactions). The entropy profile determines the extent of the convective burning shells and has significant effects on presupernova core structure and nucleosynthesis. As such it is desirable to turn on the nuclear weak reaction network as early as possible in the simulation codes and dynamically couple the network with the evolution. A sufficiently detailed and reliable nuclear reaction network (microscopically calculated taking into account the nuclear structure details of the individual nuclei) is more likely to achieve positive results.

Electron/positron captures and β^{\pm} -decay rates are amongst the most important nuclear physics inputs that determine both the Y_e and the entropy at the presupernova stage. Electron capture decreases the number of electrons available for pressure support whereas beta decay acts in the opposite direction. Both processes directly affect the overall lepton-to-baryon ratio of the core. The neutrinos and antineutrinos produced as a result of these nuclear weak reactions are transparent to the stellar matter at presupernova densities and therefore assist in cooling the core to a lower entropy state. These weak-interaction rates are required not only in the accurate determination of the structure of the stellar core but also bear significance in (explosive) nucleosynthesis and element abundance calculations. Weak interactions in presupernova stars are known to be dominated by allowed Fermi and Gamow-Teller transitions [1]. In particular, Gamow-Teller (GT) properties of nuclei in the region of medium masses around A=56 are of special importance because they are the main constituents of the stellar core in presupernova conditions.

The first ever extensive calculation of stellar weak-interaction rates was performed by Fuller, Fowler and Newmann [2]. These pioneering calculations included rates for electron/positron capture, electron/positron decay and associated (anti)neutrino energy losses for around 226 nuclei with masses between A=21 and 60. The authors also incorporated all experimental data available at that time. The GT strength distributions and excitation energies were calculated using a zero-order shell model. Aufderheide and collaborators [3] stressed on the importance of beta decay in the iron core just prior to the collapse of the core and extended the calculations [2] for heavier nuclei with A>60. Later experimental results [4–7] revealed the misplacement of the GT centroid adopted in the parameterizations of Ref. [2] and subsequently used in the calculation by Ref. [3]. Since then considerable efforts were made on the microscopic calculation of these weak-interaction rates. Large-scale shell model (hereafter LSSM)(e.g. [8]) and the proton-neutron quasiparticle random phase approximation (hereafter pn-QRPA) theory (e.g. [9]) were two of the most successful and extensively used models for the microscopic calculation of stellar weak rates.

The pn-QRPA theory is an efficient way to generate GT strength distributions. These

strength distributions constitute a primary and nontrivial contribution to the capture and decay rates among iron-regime nuclide. Nabi and Klapdor-Kleingrothaus used the pn-QRPA theory, for the first time, to calculate the weak-interaction rates over a wide range of temperature and density scale for sd- [9] and fp/fpg-shell nuclei [10] in stellar matter. Since then these calculations were refined and further improved with use of more efficient algorithms, computing power, incorporation of latest data from mass compilations and experimental values, and fine-tuning of model parameters (e.g. Refs. [11–13]). The reliability of pn-QRPA calculation was established and discussed in detail in Ref. [10]. The associated uncertainties involved in the calculations were highlighted in Ref. [14]. In this paper I use this established and improved model (as also explained later) to calculate the weak-interaction rates for key iron isotopes in presupernova conditions.

The weak decay rate from the ith state of the parent to the jth state of the daughter nucleus is given by

$$\lambda_{ij} = \ln 2 \frac{f_{ij}(T, \rho, E_f)}{(ft)_{ij}},\tag{1}$$

where (f_{ij}) are the phase space integrals and are functions of temperature (T), density (ρ) and Fermi energy (E_f) . The pn-QRPA model is employed to calculate the $(ft)_{ij}$ values for the transitions which are directly related to the reduced transition probabilities of the Fermi and GT transitions. The total weak-interaction rate per unit time per nucleus is finally given by performing a double summation of the type

$$\lambda = \sum_{ij} P_i \lambda_{ij}. \tag{2}$$

The summation was carried out over all parent and daughter states until satisfactory convergence in the rate calculation was achieved. Here P_i is the probability of occupation of parent excited states and follows the normal Boltzmann distribution. The detailed formalism may be found in Ref. [10]. The pn-QRPA theory allows a microscopic state-by-state calculation of both sums present in eq. (2). In other words the pn-QRPA model calculates the GT strength distribution of all parent excited states in a microscopic fashion. This salient feature of the pn-QRPA model greatly increases the reliability of the calculated rates in stellar matter where there exists a finite probability of occupation of parent excited states. Other models revert to approximations like 'Brink's hypothesis' (in electron capture direction) and 'back resonances' (in β -decay direction) in order to perform these summations. Brink's hypothesis states that GT strength distribution on excited states is identical to that from ground state, shifted only by the excitation energy of the state. GT back resonances are the states reached by the strong GT transitions in the inverse process (electron capture) built on ground and excited states.

Three key isotopes of iron, 54,55,56 Fe, were chosen for the calculation of GT_{\pm} strength distributions and associated weak rates using the pn-QRPA model. Reasonable experimental data were available for the even-even isotopes of iron (54,56 Fe) to test the model. Low-lying parent excited states of iron isotopes (specially 55 Fe) have a finite probability of occupation under stellar conditions and a microscopic calculation of GT_{\pm} strengths from these excited states is desirable. The pn-QRPA model is specially designed to perform this task. Aufderheide and collaborators [3] ranked 54,55,56 Fe amongst the most influential nuclei with respect to their importance for the electron capture process for the early presupernova collapse. Later Heger et al. [15] studied the presupernova evolution of massive stars and rated 54,55,56 Fe amongst the very important nuclei considered to be most important for decreasing Y_e during the oxygen and silicon burning phases. Besides, 55 Fe was also found to be in the top five list of nuclei that increases Y_e via positron capture and electron decay during the silicon burning phases [15]. The rationale behind this project is to present an alternate microscopic and accurate estimate of weak-interaction mediated rates on iron isotopes, on a detailed temperature-density grid suitable for interpolation purposes, for the

collapse simulators which may be used as a reliable source of nuclear physics input in the simulation codes.

The pn-QRPA calculation performed in this project was further improved by an optimum choice of model parameters and incorporation of latest experimental data. Recent study by Stetcu and Johnson [16] stressed particularly on the importance of deformation parameter in the QRPA model for improved results. Rather than incorporating deformations calculated from some theoretical mass model (as used in earlier calculations of pn-QRPA rates [9, 10]), for the first time the experimentally adopted value of the deformation parameter for ^{54,56}Fe, taken from Raman et al. [17], was employed in the calculation. The better choice of model parameters resulted in an improved agreement of the calculated centroids of the GT strength distributions with measurements. The GT₊ centroid for ⁵⁴Fe (⁵⁶Fe) was improved from 6.29 MeV (4.68 MeV) to 4.06 MeV (3.13 MeV). The corresponding measured centroids are $3.7 \pm$ $0.2 \text{ MeV} (2.9 \pm 0.2 \text{ MeV})$. The total calculated strengths $\Sigma S_{\beta^{\pm}}$ were also in better agreement with the measured values (see Table 1). For the case of ⁵⁵Fe (where measurement lacks) the deformation of the nucleus was calculated using the mass compilation of Möller and Nix [18]. In order to further increase the reliability of the calculated weak rates experimental data were incorporated in the calculation wherever possible. For details see Ref. [13]. A stateby-state calculation of GT_{\pm} strength was performed for a total of 246 parent excited states in ⁵⁴Fe, 297 states in ⁵⁵Fe and 266 states in ⁵⁶Fe. For each parent excited state, transitions were calculated for a total of 150 daughter excited states. The band width of energy states was chosen accordingly to cover an excitation energy range of (15 - 20) MeV in parent and daughter. The summations in eq. (2) were done to ensure satisfactory convergence. The use of a separable interaction assisted in the incorporation of a luxurious model space of up to 7 major oscillator shells which in turn made possible to consider these many excited states both in parent and daughter nuclei (interested readers are referred to Ref. [10] for details of the model description).

Both β -decay and capture rates are very sensitive to the location of the GT_+ centroid [19]. An overall quenching factor of 0.6 [20] was adopted in the current pn-QRPA calculation of GT strength in both directions for all iron isotopes. A considerable amount of uncertainty is present in the calculations and measurements of GT strength distribution. The associated uncertainties in the pn-QRPA model was discussed in Ref. [14]. Table 1 displays the comparison of the calculated GT centroids and total strengths $(\Sigma S_{\beta^{\pm}})$ against measurement, LSSM calculation and earlier pn-QRPA calculation of Ref. [10] for ^{54,56}Fe. For the case of ⁵⁴Fe (⁵⁶Fe) the value of total S_{β^+} was taken from Ref. [4] (Ref. [5]) whereas the total measured S_{β^-} strength was taken from Ref. [6] (Ref. [7]). The pn-QRPA calculated total strengths, ΣS_{β^+} , lie closer to the upper bound of the measured values. The calculated ΣS_{β^-} strengths match very well with the measurements. The calculated weak rates are sensitive to the location of GT₊ centroids [19]. The pn-QRPA centroids are within the upper range of the measured values and are placed at relatively higher energies in daughter nuclei as compared to LSSM numbers. Experimental (p,n) data are also available for ^{54,56}Fe. According to Anderson and collaborators [6] the amount of GT strength in the background and continuum remained highly uncertain. For ⁵⁴Fe (⁵⁶Fe) the centroid of the data of discrete peaks [6] ([7]) was calculated to be 7.63 MeV (8.27 MeV). The pn-QRPA calculated values are 5.08 MeV and 5.61 MeV, respectively. Despite greater experimental certainties in the (p,n) data one notes that the pn-QRPA places the centroid at much lower energies in daughter nuclei as compared to measurements. However it is to be noted that the total strengths (in both direction) compare very well with the measured values. Also the location of GT₊ centroids is in very good agreement with the measured data which is mainly responsible for the calculation of weak rates on iron isotopes [19]. The Ikeda sum rule was satisfied for the ground states of iron isotopes for the unquenched values in the calculation for the complete range of excitation energies covered in daughter nuclei as discussed above. (Note that the values of the total $S_{\beta^{\pm}}$ strengths given later in Table 1 and Table 2 are calculated up to an excitation energy of 12MeV in daughter.) For reasons not known to the author, LSSM did not present the location of GT₋ centroids in their paper [8]. Table 1 also highlights the improvement in the current calculation as compared to the pn-QRPA calculation of Ref. [10].

Table 2 basically shows that the Brink's hypothesis (also used in the LSSM calculation) may not be a good approximation to use in calculation of stellar weak rates for iron isotopes. The energies in parenthesis are experimental. The centroids of the GT_{\pm} strength distributions are shifted to higher excitation energies in daughter nuclei for the parent excited states as compared to the ground state centroids. The total strengths $S_{\beta^{\pm}}$ also change appreciably for the excited states. These changes have an effect on the calculated weak rates specially at low temperatures and densities (where specific low-lying transitions may dominate the rate calculation).

The cumulative GT_+ strength distributions for the iron isotopes are presented in fig. 1. The insets show the corresponding experimental results. For the case of 55 Fe where no measurement is available, the summed GT_- strength distribution is shown instead in the inset. As can be seen from fig. 1, the calculated distributions are fragmented, well spread and are in good agreement with the measured distributions.

The calculated weak rates for the iron isotopes during presupernova evolution from postoxygen burning till the presupernova model for massive stars are depicted in figs. 2, 3 and 4 (color online). Each figure consists of three panels of increasing presupernova density and depicts six weak-interaction rates calculated using the pn-QRPA model at astrophysically relevant temperature and density scales. These include electron capture (ec), positron decay (pd), neutrino energy losses (neu), positron capture (pc), electron decay (ed) and antineutrino energy loss rates (aneu) for ^{54,55,56}Fe. All weak rates are given in log to base 10 scales. The capture and decay rates (open markers) are given in units of s^{-1} whereas the neutrino and antineutrino energy losses (filled upper triangle and star, respectively) are given in units of $MeVs^{-1}$. In these figures T_9 gives the stellar temperature in units of 10^9 K. It may be noted from these figures that electron capture, positron decay and neutrino energy losses are more dominant than the other three weak-interaction processes specially at low temperatures. Furthermore the electron capture rates and neutrino energy losses on one hand and the electron decay (also positron capture) rates and antineutrino energy losses on the other hand are fairly similar in magnitude during the presupernova evolution of massive stars. These figures also imply that during this time period the electron capture and neutrino cooling rates are the dominant weak-processes and hence most important for core-collapse simulators.

How does the pn-QRPA calculated rates compare with the LSSM results during the presupernova evolution of massive stars? The answer is given in tables 3, 4. These tables show the comparison of weak rate calculations in astrophysically relevant regions (as determined by the studies of presupernova evolution of massive stars by Ref. [15]). In these tables T_9 gives the stellar temperature in units of 10^9 K and ρ_7 is the density in units of $10^7 gcm^{-3}$. In table 3, R_{ec} and R_{pd} are the ratios of pn-QRPA calculated electron capture and positron decay rates to those calculated using LSSM (in this direction Fe isotopes transform to Mn). As discussed above the electron capture rates are much bigger (by many orders of magnitude) than the competing positron decay rates and hence are more important for core-collapse simulators. The neutrino produced as a result of these two weak processes are transparent to the stellar matter during the presupernova evolution of massive stars and their cooling capability is determined by the neutrino energy loss rates and R_{ν} gives the corresponding pn-QRPA to LSSM calculated ratio. For all isotopes of iron the pn-QRPA calculated electron capture and neutrino energy losses are in very good agreement with the LSSM rates. Positron decay rates are much smaller and relatively less important for simulation codes. The comparison of positron decay rates of 54,55 Fe is very good at lower temperatures ($T_9 =$ 2-3). Otherwise the pn-QRPA calculated positron decay rates are smaller by around one to two orders of magnitude.

Table 4 shows the ratios of the reported positron capture (R_{pc}) , electron decay (R_{ed}) and

antineutrino energy loss rates $(R_{\bar{\nu}})$ to LSSM rates for ⁵⁵Fe during the silicon burning phases of massive stars. Positron capture and electron decay rates are of comparable magnitudes and compete well with each other (see figures 2,3,4). The positron capture rates on ⁵⁵Fe are in reasonable agreement with the LSSM results whereas the calculated β -decay rates are smaller by three to five orders of magnitude. It was pointed out by authors in [3, 15] that β -decay rates are negligible in the presupernova model. During the silicon burning phases the pn-QRPA calculated antineutrino energy loss rates are also smaller by up to five orders of magnitude. The beta decay rates are very sensitive to the available phase space as compared to the capture rates. The phase space is given by $(Q + E_i - E_j)$ where $E_i(E_i)$ are the parent (daughter) excitation energies and Q is the Q-value of the reaction. The calculated GT strength distribution and placement of GT_ centroid caused the big suppression in the pn-QRPA β -decay rates. The centroid placement in reported calculation is given in table 2. The β -decay rates tend to go down at high densities due to the blocking of the available phase space of increasingly degenerate electrons. At high densities the contribution to the total β -decay rates by the excited states is very important, specially for higher temperatures, because such states, due to their higher available phase space, are still unblocked. The enhancement in LSSM beta decay rates may also be attributed to the inclusion of back resonances in their calculation. It is to be noted that these rates are very small numbers and can change by orders of magnitude by a mere change of 0.5 MeV, or less, in parent or daughter excitation energies, $E_i(E_i)$, and are more reflective of the uncertainties in the calculation of energies.

The aim of this paper was to present an alternate microscopic and accurate estimate of weak-interaction mediated rates on key iron isotopes for the collapse simulators. As mentioned earlier, the pn-QRPA model makes a microscopic calculation of GT strength from all parent excited states possible which greatly increases the utility of this model in calculation of stellar weak-interaction rates. The complete set of detailed calculation of all six weak rates for iron isotopes as a function of stellar temperature, density and Fermi energy, suitable for core-collapse simulations and interpolation purposes, is available as ASCII files and can be requested from the author. A detailed study of GT strength distributions and weak-interaction rates of these iron isotopes along with a comprehensive comparison with previous calculations will be presented elsewhere. The overall final lepton fraction and entropy of the collapsing core can be determined by the calculation of similar reaction rates for other important iron-regime nuclei. Work is in progress on improved calculations of pn-QRPA rates of other astrophysically important fp-shell nuclide and one can hope that in near future a microscopic, reliable and complete set of nuclear physics input will be available for the core-collapse simulators to probe for some possible interesting outcome.

* * *

The author would like to acknowledge the kind hospitality provided by the Abdus Salam ICTP, Trieste, where part of this project was completed. The author further wishes to acknowledge the comments of one of the Referee which lead to the proper incorporation of experimental data in case of calculations for 55 Fe.

REFERENCES

- Bethe H. A., Brown G. E., Applegate J. and Lattimer J. M., Nucl. Phys., A324 (1979) 487.
- Fuller G. M., Fowler W. A. and Newman M. J., Astrophys. J. Suppl. Ser, 42 (1980) 447;
 Astrophys. J. Suppl. Ser, 48 (1982) 279; Astrophys. J., 252 (1982) 715; Astrophys. J., 293 (1985) 1.
- [3] Aufderheide M. B., Fushiki I., Woosley S. E., Stanford E. and Hartmann D. H., Astrophys. J. Suppl. Ser, 91 (1994) 389.

- [4] RÖNNQVIST T., CONDÉ H., OLSSON N., RAMSTRÖM E., ZORRO R., BLOMGREN J., HÅKANSSON A., RINGBOM A., TIBELL G., JONSSON O., NILSSON L., RENBERG P.-U, VAN DER WERF S. Y., UNKELBACH W. and BRADY F. P., *Nucl. Phys.*, **A563** (1993) 225.
- [5] EL-KATEB S., JACKSON K. P., ALFORD W. P., ABEGG R., AZUMA R. E., BROWN B. A., CELLER A., FREKERS D., HÄUSSER O., HELMER R., HENDERSON R. S., HICKS K. H., JEPPESEN R., KING J. D., RAYWOOD K., SHUTE G. G., SPICER B. M., TRUDEL A., VETTERLI M. and YEN S., *Phys. Rev. C*, **49** (1994) 3128.
- [6] ANDERSON B. D., LEBO C., BALDWIN A. R., CHITTRAKARN T., MADEY R. and WATSON J. W., Phys. Rev. C, 41 (1990) 1474.
- [7] RAPAPORT J., TADDEUCCI T., WELCH T. P., GAARDE C., LARSEN J., HOREN D. J., SUGARBAKER E., KONCZ P., FOSTER C. C., GOODMAN C. D., GOULDING C. A. and MASTERSON T., Nucl. Phys., **A410** (1983) 371.
- [8] LANGANKE K. and MARTÍNEZ-PINEDO G., Nucl. Phys., A673 (2000) 481.
- [9] Nabi J.-Un and Klapdor-Kleingrothaus H. V., At. Data Nucl. Data Tables, 71 (1999) 149.
- [10] Nabi J.-Un and Klapdor-Kleingrothaus H. V., At. Data Nucl. Data Tables, 88 (2004) 237.
- [11] Nabi J.-Un and Rahman M.-Ur., Phys. Rev. C, 75 (2007) 035803.
- [12] Nabi J.-Un and Sajjad M., Phys. Rev. C, 76 (2007) 055803.
- [13] Nabi J.-Un, Phys. Rev. C, 78 (2008) 045801.
- [14] Nabi J.-Un and Sajjad M., Phys. Rev. C, 77 (2008) 055802.
- [15] HEGER A., WOOSLEY S. E., MARTÍNEZ-PINEDO G. and LANGANKE K., Astrophys. J., 560 (2001) 307.
- [16] STETCU I. and JOHNSON C. W., Phys. Rev. C, 69 (2004) 024311.
- [17] RAMAN S., MALARKEY C. H., MILNER W. T., NESTOR, JR. C. W. and STELSON P. H., At. Data Nucl. Data Tables, 36 (1987) 1.
- [18] MÖLLER P. and NIX J. R., At. Data Nucl. Data Tables, 26 (1981) 165.
- [19] AUFDERHEIDE M. B., BLOOM S. D., MATHEWS G. J. and RESLER D. A., Phys. Rev. C, 53 (1996) 3139.
- [20] Gaarde C., Nucl. Phys., A396 (1983) 127c.

Table 1: Comparison of measured GT₊ centroids and total $S_{\beta^{\pm}}$ strengths with microscopic calculations of the improved pn-QRPA model (this work), large scale shell model (LSSM) [8] and those of Ref. [10] in $^{54}Fe(^{56}Fe)$. For experimental references see text.

| Source | $E(GT_+)$ | ΣS_{β} | ΣS_{β}^{+} |
|------------|------------------------|------------------------|------------------------|
| Experiment | $3.7\pm0.2(2.9\pm0.2)$ | $7.5\pm0.7(9.9\pm2.4)$ | $3.5\pm0.7(2.9\pm0.3)$ |
| pn-QRPA | 4.06(3.13) | 7.56(10.74) | 4.26(3.71) |
| LSSM | 3.78(2.60) | 7.11(9.80) | 3.56(2.70) |
| Ref. [10] | 6.29(4.68) | 9.47(12.47) | 4.49(4.72) |

Table 2: Comparison of pn-QRPA calculated centroids $E(GT_{\pm})$ and total $S_{\beta^{\pm}}$ strengths for the ground and first two excited states of $^{54,55,56}Fe$. The cut-off energy in daughter nuclei is 12 MeV.

| States | $E(GT_+)[MeV]$ | $E(GT_{-})[MeV]$ | ΣS_{β} + | ΣS_{β} |
|----------------------------|----------------|------------------|----------------------|--------------------|
| $^{54}Fe~(0.0~{\rm MeV})$ | 4.06 | 5.08 | 4.26 | 7.56 |
| $^{54}Fe~(1.41~{\rm MeV})$ | 7.10 | 7.81 | 5.12 | 6.97 |
| $^{54}Fe~(2.56~{\rm MeV})$ | 7.48 | 8.23 | 3.84 | 9.23 |
| $^{55}Fe~(0.0~{\rm MeV})$ | 7.12 | 8.28 | 4.68 | 6.87 |
| $^{55}Fe~(0.41~{\rm MeV})$ | 7.38 | 8.56 | 4.43 | 8.87 |
| $^{55}Fe~(0.93~{\rm MeV})$ | 7.40 | 8.83 | 5.03 | 6.87 |
| $^{56}Fe~(0.0~{\rm MeV})$ | 3.13 | 5.61 | 3.71 | 10.74 |
| $^{56}Fe~(0.85~{\rm MeV})$ | 6.17 | 8.89 | 5.15 | 8.04 |
| $^{56}Fe~(2.08~{\rm MeV})$ | 6.74 | 8.76 | 4.15 | 10.21 |

Table 3: Ratios of pn-QRPA weak rates to those calculated using LSSM [8] in presupernova conditions for key iron isotopes. See text for explanation of symbols.

| | | $T_9 = 2$ | | l | $T_9 = 3$ | |
|---|--|--|--|--|--|--|
| 54 Fe | R_{ec} | R_{pd} | R_{ν} | R_{ec} | R_{pd} | R_{ν} |
| $\rho_7 = 1$ | 3.26E+00 | 1.33E+00 | 3.59E+00 | 2.38E+00 | 6.37E-01 | 2.47E + 00 |
| $\rho_7 = 10$ | 3.40E+00 | 1.33E+00 | 3.23E+00 | 2.26E+00 | 6.37E-01 | 2.27E + 00 |
| $\rho_7 = 100$ | 1.17E+00 | 1.33E+00 | 1.41E+00 | 1.11E+00 | 6.37E-01 | 1.31E+00 |
| $^{55}\mathrm{Fe}$ | | | | | | |
| $\rho_7 = 1$ | 1.09E+00 | 1.57E + 00 | 1.10E+00 | 1.44E+00 | 1.40E + 00 | 1.49E + 00 |
| $\rho_7 = 10$ | 1.81E+00 | 1.57E + 00 | 1.43E+00 | 1.63E+00 | 1.40E+00 | 1.53E + 00 |
| $\rho_7 = 100$ | 1.26E+00 | 1.57E+00 | 1.59E+00 | 1.06E+00 | 1.40E+00 | 1.31E+00 |
| $^{56}\mathrm{Fe}$ | | | | | | |
| $\rho_7 = 1$ | 1.14E+00 | 1.77E-01 | 1.07E+00 | 1.17E + 00 | 7.80E-02 | 1.08E + 00 |
| $\rho_7 = 10$ | 1.35E+00 | 1.77E-01 | 1.32E+00 | 1.37E+00 | 7.78E-02 | 1.29E+00 |
| $\rho_7 = 100$ | 2.11E+00 | 1.77E-01 | 1.97E + 00 | 1.80E + 00 | 7.78E-02 | 1.71E + 00 |
| | | | | | | |
| | | $T_9 = 5$ | | | $T_9 = 10$ | |
| | | | | | | |
| ⁵⁴ Fe | R_{ec} | R_{pd} | R_{ν} | R_{ec} | R_{pd} | R_{ν} |
| $\rho_7 = 1$ | R_{ec} 1.39E+00 | | R_{ν} 1.31E+00 | R_{ec} 9.95E-01 | - | $R_{\nu} \\ 8.34\text{E-}01$ |
| $ \rho_7 = 1 \\ \rho_7 = 10 $ | | R_{pd} | 1.31E+00 1.36E+00 | 9.95E-01 9.91E-01 | R_{pd} | |
| $ \rho_7 = 1 \rho_7 = 10 \rho_7 = 100 $ | 1.39E+00 | R_{pd} 2.29E-01 | 1.31E + 00 | 9.95E-01 | R_{pd} 1.07E-01 | 8.34E-01 |
| $ \rho_7 = 1 \\ \rho_7 = 10 $ | 1.39E+00 1.35E+00 | R_{pd} 2.29E-01 2.31E-01 | 1.31E+00 1.36E+00 | 9.95E-01 9.91E-01 | R_{pd} 1.07E-01 1.10E-01 | 8.34E-01 8.97E-01 |
| $ \rho_7 = 1 \rho_7 = 10 \rho_7 = 100 $ | 1.39E+00 1.35E+00 | R_{pd} 2.29E-01 2.31E-01 | 1.31E+00 1.36E+00 | 9.95E-01 9.91E-01 9.12E-01 1.12E+00 | R_{pd} 1.07E-01 1.10E-01 | 8.34E-01 8.97E-01 |
| $ \rho_7 = 1 \rho_7 = 10 \rho_7 = 100 $ 55 Fe $ \rho_7 = 1 \rho_7 = 10 $ | 1.39E+00 1.35E+00 9.93E-01 | R_{pd} 2.29E-01 2.31E-01 2.31E-01 | 1.31E+00 1.36E+00 1.10E+00 1.79E+00 1.72E+00 | 9.95E-01 9.91E-01 9.12E-01 1.12E+00 1.09E+00 | $\begin{array}{c} R_{pd} \\ 1.07\text{E-}01 \\ 1.10\text{E-}01 \\ 1.11\text{E-}01 \\ \end{array}$ $\begin{array}{c} 7.36\text{E-}02 \\ 7.76\text{E-}02 \\ \end{array}$ | 8.34E-01 8.97E-01 9.31E-01 |
| $ \rho_7 = 1 \rho_7 = 10 \rho_7 = 100 $ 55 Fe $ \rho_7 = 1 \rho_7 = 10 \rho_7 = 100 $ | 1.39E+00 1.35E+00 9.93E-01 1.75E+00 | R_{pd} 2.29E-01 2.31E-01 2.31E-01 6.43E-01 | 1.31E+00 1.36E+00 1.10E+00 1.79E+00 | 9.95E-01 9.91E-01 9.12E-01 1.12E+00 | R_{pd} 1.07E-01 1.10E-01 1.11E-01 7.36E-02 | 8.34E-01 8.97E-01 9.31E-01 1.02E+00 |
| $ \rho_7 = 1 \rho_7 = 10 \rho_7 = 100 $ 55 Fe $ \rho_7 = 1 \rho_7 = 10 $ | 1.39E+00 1.35E+00 9.93E-01 1.75E+00 1.58E+00 | $\begin{array}{c} R_{pd} \\ 2.29 \text{E-}01 \\ 2.31 \text{E-}01 \\ 2.31 \text{E-}01 \\ 2.31 \text{E-}01 \\ 6.43 \text{E-}01 \\ 6.44 \text{E-}01 \\ \end{array}$ | 1.31E+00 1.36E+00 1.10E+00 1.79E+00 1.72E+00 | 9.95E-01 9.91E-01 9.12E-01 1.12E+00 1.09E+00 | $\begin{array}{c} R_{pd} \\ 1.07\text{E-}01 \\ 1.10\text{E-}01 \\ 1.11\text{E-}01 \\ \end{array}$ $\begin{array}{c} 7.36\text{E-}02 \\ 7.76\text{E-}02 \\ \end{array}$ | 8.34E-01 8.97E-01 9.31E-01 1.02E+00 1.07E+00 |
| $ \rho_7 = 1 \rho_7 = 10 \rho_7 = 100 $ 55 Fe $ \rho_7 = 1 \rho_7 = 10 $ $ \rho_7 = 100 $ | 1.39E+00 1.35E+00 9.93E-01 1.75E+00 1.58E+00 | $\begin{array}{c} R_{pd} \\ 2.29 \text{E-}01 \\ 2.31 \text{E-}01 \\ 2.31 \text{E-}01 \\ 2.31 \text{E-}01 \\ 6.43 \text{E-}01 \\ 6.44 \text{E-}01 \\ \end{array}$ | 1.31E+00 1.36E+00 1.10E+00 1.79E+00 1.72E+00 | 9.95E-01 9.91E-01 9.12E-01 1.12E+00 1.09E+00 | $\begin{array}{c} R_{pd} \\ 1.07\text{E-}01 \\ 1.10\text{E-}01 \\ 1.11\text{E-}01 \\ \end{array}$ $\begin{array}{c} 7.36\text{E-}02 \\ 7.76\text{E-}02 \\ \end{array}$ | 8.34E-01 8.97E-01 9.31E-01 1.02E+00 1.07E+00 |
| $\begin{array}{c} \rho_{7} = 1 \\ \rho_{7} = 10 \\ \rho_{7} = 100 \\ \hline \\ {}^{55}\text{Fe} \\ \rho_{7} = 1 \\ \rho_{7} = 10 \\ \hline \\ {}^{56}\text{Fe} \end{array}$ | 1.39E+00 1.35E+00 9.93E-01 1.75E+00 1.58E+00 8.75E-01 | R_{pd} 2.29E-01 2.31E-01 2.31E-01 6.43E-01 6.44E-01 | 1.31E+00 1.36E+00 1.10E+00 1.79E+00 1.72E+00 1.12E+00 | 9.95E-01 9.91E-01 9.12E-01 1.12E+00 1.09E+00 8.55E-01 | R_{pd} 1.07E-01 1.10E-01 1.11E-01 7.36E-02 7.76E-02 7.91E-02 | 8.34E-01 8.97E-01 9.31E-01 1.02E+00 1.07E+00 9.89E-01 |

Table 4: Ratios of pn-QRPA weak rates to those calculated using LSSM [8] in presupernova conditions for ^{55}Fe . See text for explanation of symbols.

| | $T_9 = 2$ | | | $T_9 = 3$ | | | $T_9 = 5$ | | |
|------------------|-----------|----------|-----------------|-----------|----------|-----------------|-----------|----------|-----------------|
| ⁵⁵ Fe | R_{pc} | R_{ed} | $R_{\bar{\nu}}$ | R_{pc} | R_{ed} | $R_{\bar{\nu}}$ | R_{pc} | R_{ed} | $R_{\bar{\nu}}$ |
| $\rho_7 = 1$ | 1.52E-01 | 2.47E-03 | 1.45E-02 | 4.72E-01 | 5.92E-04 | 2.89E-02 | 7.01E-01 | 1.54E-04 | 1.22E-01 |
| $\rho_7 = 10$ | 1.52E-01 | 8.51E-05 | 6.37E-04 | 4.72E-01 | 4.61E-05 | 2.61E-03 | 7.00E-01 | 4.61E-05 | 2.08E-02 |
| $\rho_7 = 100$ | 1.52E-01 | 2.11E-05 | 1.79E-04 | 4.71E-01 | 1.27E-05 | 7.96E-04 | 7.00E-01 | 1.79E-05 | 6.58E-03 |

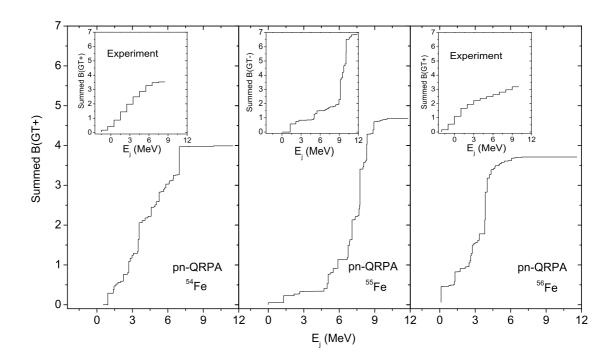


Fig. 1: Cumulative Gamow-Teller (GT_+) strength distributions for iron isotopes. The inset depicts experimental results. For 55 Fe (middle panel) the inset shows the summed B(GT_-) strength distribution.

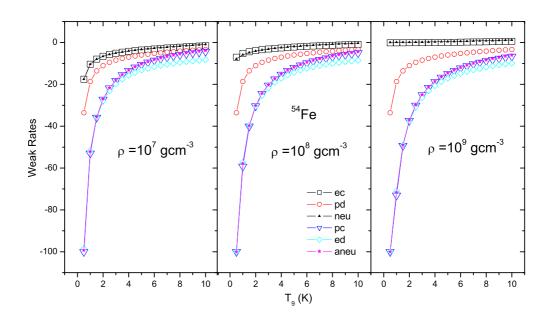


Fig. 2: (Color online) Weak-interaction rates for 54 Fe during presupernova evolution of massive stars calculated using the pn-QRPA theory. Here ec, pd, neu, pc, ed and aneu stand for calculated electron capture, positron decay, neutrino energy loss, positron capture, electron decay and antineutrino energy loss rates, respectively. For units of calculated weak rates see text.

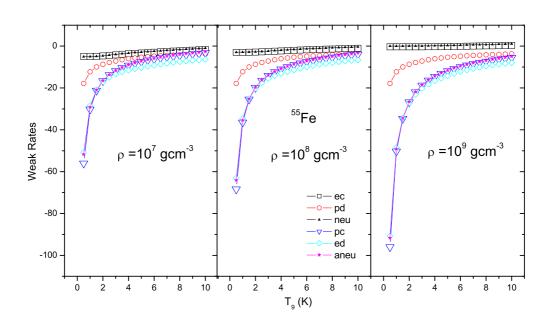


Fig. 3: (Color online) Same as fig. 2 but for $^{55}\mathrm{Fe}.$

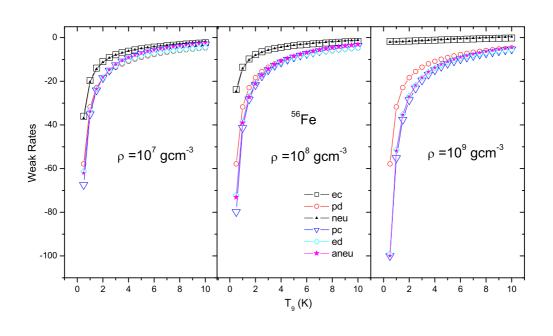


Fig. 4: (Color online) Same as fig. 2 but for 56 Fe.